START PAGE

Chapter 7

CLOSED-LOOP MOTION CONTROL IN ELECTRIC DRIVES

7.1. INTRODUCTION

By motion control we mean torque, speed or position control. Motion control systems are characterized by precision, response quickness and immunity to parameter detuning, torque and inertia perturbations and energy conversion rates. Motion control through electric motors and power electronic converters (PECs) may be approached by the theory and practice of linear and nonlinear, continuous or discrete control systems. Control systems is a field of science in itself and in what follows only a few solutions of practical interest for motion control will be introduced with some application examples, from simple to complex.

To simplify the treatment and to include the PM d.c. brush motor control, the latter will be considered for various motion control systems. PM d.c. brush motors are characterized by a low electrical time constant, τ_e = L/R, of a few milliseconds or less. The armature (torque) current is fully decoupled from the PM field because of the orthogonality of the armature and PM fields, both at standstill and for any rotor speed.

As shown in later chapters, vector control of a.c. motors also decouples flux and torque control if the orientation to the flux linkage is secured and flux amplitude is kept constant. Consequently, vector controlled a.c. motors are similar to d.c. brush motors and thus the application of various motion control systems to the d.c. motor holds notable generality while also eliminating the necessity of a separate chapter on closed-loop control of brushless motors.

To start with, the cascaded motion linear control is presented through numerical examples.

7.2. THE CASCADED MOTION CONTROL

A typical motion control system comprises three loops: one for torque, one for speed and one for position (Figure 7.1.). Ideally the system has independent position and speed sensors though, in general, only one is used — the speed sensor for speed control and the position one for position control — with the speed in the latter case estimated from the position information.

The PM d.c. brush motor equations are

$$V = Ri + L\frac{di}{dt} + \lambda_{PM}\omega_r \tag{7.1}$$

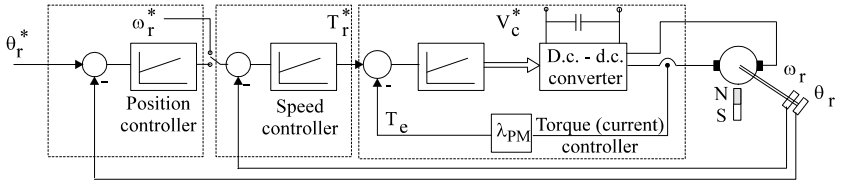

Figure 7.1. Typical cascaded motion control

$$J\frac{d\omega_r}{dt} = T_e - T_L \tag{7.2}$$

$$\frac{d\theta_r}{dt} = \omega_r \tag{7.3}$$

$$T_e = \lambda_{PM} I \tag{7.4}$$

7.2.1. The torque loop

The torque control for constant flux linkage (λ_{PM}) means (with core loss neglected) armature current control for a PM d.c. brush motor. Fast current control also provides for fast current protection. The design of the torque loop implies knowing the load torque T_L. Alternatively, T_L = constant and, after the design is completed, the influence of load torque perturbations on loop stability is investigated and adequate corrections added, if required.

For constant (or zero) load torque the PM d.c. brush motor current / voltage transfer function, from (7.1)-(7.4), becomes (see eqn. 4.43):

$$H_V(s) = \frac{i(s)}{V(s)} = \frac{s\tau_{em}}{\left(s^2\tau_{em}\tau_e + s\tau_{em} + 1\right)R} \tag{7.5}$$

where

$$\tau_{em} = \frac{JR}{\lambda_{PM}^2} \tag{7.6}$$

is the electromechanical time constant of the motor.

The superaudible frequency chopper may be modeled through its gain K_c as its delay may be neglected. The torque constant $K_T = T_e / I = \lambda_{PM}$ and the current sensor amplification is K_I.

The typical torque controller is PI type with the gain K_{SI} and the time constant τ_{si}. The block diagram is shown in Figure 7.2. The theory of linear

systems offers numerous design approaches to PI controllers [1] both for continuous and discrete implementation.

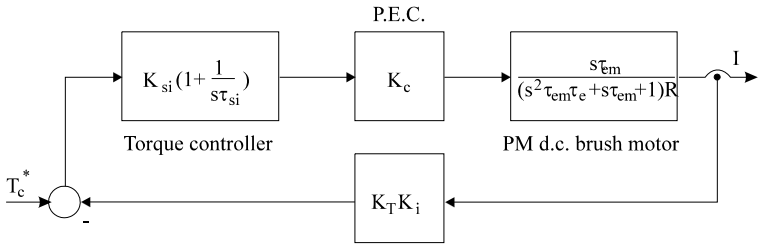

Figure 7.2. PI torque loop for a PM d.c. brush motor

In what follows we are using the critical frequency ω_c and phase margin φ_c constraints for the open-loop transfer function A(s) of the system in Figure 7.2.

$$A(s)=\frac{K_{si}(1+s\tau_{si})}{s\tau_{si}R}\frac{K_CK_TK_Is\tau_{em}}{s^2\tau_{em}\tau_e+s\tau_{em}+1} \tag{7.7}$$

The critical frequency ω_c should be high — up to 1...2 kHz — to provide fast torque (current) control.

Let us take as a numerical example a PM d.c. brush motor with the data: V_n = 110 V, P_n = 2 kW, n_n = 1800 rpm, R = 1 Ω, L = 20 mH, K_T = 1.1 Nm/A, τ_{em} = 0.1 sec., K_C = 25 V/V, K_i = 0.5 V/A, critical frequency f_c = 500 Hz, and the phase margin φ_c = 47°.

The phase margin φ_c of A(s) from (7.7), for the critical frequency $\omega_c = 2\pi f_c$, is

$$\begin{aligned}\varphi_c &= -180^\circ+\text{Arg}[A(j\omega_c)]=\\ &=-180^\circ+\tan^{-1}(\omega_c\tau_{si})-\tan^{-1}\left(\frac{\omega_c\tau_{em}}{1-\omega_c{}^2\tau_{em}\tau_e}\right)\end{aligned} \tag{7.8}$$

Consequently

$$\tan^{-1}(\omega_c\tau_{si})=180^\circ+47^\circ+\tan^{-1}\frac{2\pi500\cdot0.1}{1-(2\pi500)^2\cdot0.1\cdot0.02}=46^\circ \tag{7.9}$$

And thus,

$$\tau_{si}=\frac{\tan 46^\circ}{2\pi500}=0.3075 \text{ ms} \tag{7.10}$$

The gain of the torque controller K_{si} may be calculated from the known condition:

$$\left|A\left(j\omega_c\right)\right| = 1 \tag{7.11}$$

Finally,

$$K_{si} = \frac{0.3075\cdot 10^{-3}\cdot 1}{25\cdot 1.1\cdot 0.5\cdot 0.1}\cdot\sqrt{\frac{\left(10^3\pi 0.1\right)^2+\left(1-10^6\pi^2 0.1\cdot 0.01\right)^2}{1+0.965^2}} = 2.205 \tag{7.12}$$

7.2.2. The speed loop

In numerous applications, speed control is required. The torque loop is still there to limit the current, quicken the response and reduce the gain in the current loop. The block diagram of a system for speed control, with the torque (current) loop included, is shown in Figure 7.3.

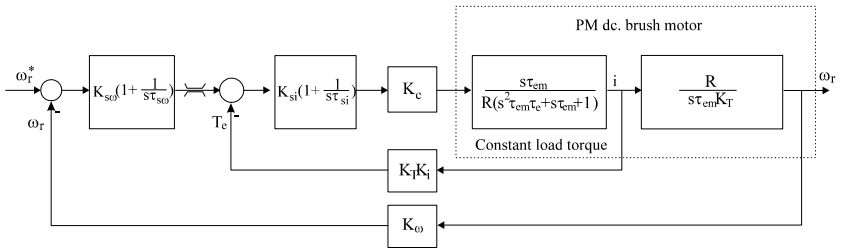

Figure 7.3. Speed control with torque (current) inner loop

Assuming that the torque loop has been already designed as above, only the speed-loop design will be discussed here. The block diagram in Figure 7.3 may be restructured as in Figure 7.4, where K_ω is the gain of the speed sensor.

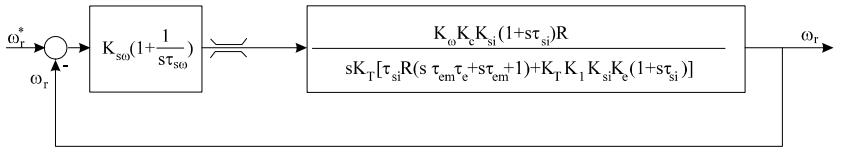

Figure 7.4. Simplified speed-loop block diagram

For the speed-loop design we may proceed as above for the torque loop, but with a critical frequency $f_{c\omega} = 100$Hz and a phase margin $\varphi_{c\omega} = 60°$ with $K_\omega = 0.057$ V sec/rad. The final results are $\tau_{s\omega} = 2.87$ ms and $K_{s\omega} = 2.897\cdot 10^3$. The amplification $K_{s\omega}$ is rather high but the phase margin is ample

and produces a reasonably low overshoot and well-damped oscillatory response.

In a similar manner we may proceed to design and add the position loop for completion of the cascaded controller. It is known that such cascaded linear controllers do not excel in terms of robustness to parameter, inertia or load changes. Additional measures are required, and they will be treated later in this chapter.

For now, however, we are treating the digital position control through a single digital filter rather than a cascaded controller, to broaden the spectrum of motion control practical approaches.

7.2.3. Digital position control

The basic configuration of a digital position control system is shown in Figure 7.5.

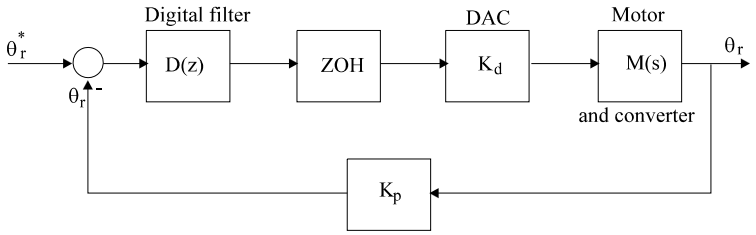

Figure 7.5. Basic digital position control system

Figure 7.5 features the motor-converter transfer function, a digital-analog converter (DAC), a sample-and-hold (ZOH) and digital filter D(z) which represents, in fact, the position controller. Only position feedback is included as obtained from an encoder with N pulses per revolution which, through the division of the two 90° phase-shifted pulse trains, produces 4N pulses per revolution and a bit for motion direction.

Suppose only an 8-bit DAC with $V_d = \pm 10V$ is used. Consequently its amplification K_d is

$$K_d = \frac{2V_d}{2^n} = \frac{20}{2^8} = \frac{20}{256} \text{ V/pulse} \tag{7.13}$$

The amplification of the encoder K_p is

$$K_p = \frac{4N}{2\pi} \text{ pulse / rad} \tag{7.14}$$

The position control is performed in a DSP with the discretization period of T. The position error $\varepsilon(KT)$ is

$$\varepsilon(KT) = \theta_r^*(KT) - \theta_r(KT) \tag{7.15}$$

The position controller filters this error to produce the command Y(KT) which is periodically applied through the DAC

$$V_C = K_d \cdot Y(KT) \tag{7.16}$$

The command voltage V_c is kept constant during the discretization period T, the effect being known as ZOH. The digital filter may be expressed by finite difference equations of the type [2]

$$Y(KT) = 2\varepsilon(KT) - \varepsilon\big((K-1)T\big) \tag{7.17}$$

z-transform may be used to model (7.17). The z-transform shifting property is

$$f(K-m) \to z^{-m} f(z) \quad \text{with } f(K) \to f(z) \tag{7.18}$$

Consequently, (7.17) becomes

$$Y(z) = 2\varepsilon(z) - z^{-1}\varepsilon(z) \tag{7.19}$$

The D(z) is thus

$$D(z) = \frac{Y(z)}{\varepsilon(z)} = \frac{2z-1}{z} \tag{7.20}$$

Let us now prepare for a numerical example by specifying the PM d.c. brush motor-converter transfer function with the electrical time constant τ_e neglected as it is very low for an axial airgap configuration motor, for example,

$$M(s) = \frac{\theta_s(s)}{V_C(s)} = \frac{K_c}{s(1+s\tau_{em})K_T} \tag{7.21}$$

The data for this new numerical example are K_T = 0.2Nm/A, R = 1Ω, L = 0H, J = 4×10^{-3} kgm^2, K_c = 10 V/V with the critical frequency ω_c = 125 rad/sec and the phase margin φ_{cp} = 45°.

The problem may be solved adopting a continual filter (controller) and finally "translating" it into a discrete form.

The motor-converter transfer function M(s) is

$$M(s) = \frac{50}{s(1+s\cdot 0.1)};\quad \tau_{em} = \frac{RJ}{K_T{}^2} = \frac{1\times 4\times 10^{-3}}{0.2^2} = 0.1\,\text{s} \tag{7.22}$$

The DAC amplification is K_d = 10/128 (8 bit). The encoder produces N = 500 pulses/revolution, which provides in fact 4N = 2000 pulses/revolution, and has the amplification K_p

$$K_p = \frac{4N}{2\pi} = \frac{2000}{2\pi} = 318 \text{ pulses / rad} \tag{7.23}$$

The discretization (sampling) time is $T = 10^{-3}$ sec. Thus the ZOH transfer function is

$$ZOH(s) \approx e^{-\frac{sT}{2}} = e^{-s\cdot 5\cdot 10^{-4}} \tag{7.24}$$

The various transfer functions in Figure 7.5 are united in a unique transfer function H(s)

$$H(s) = K_d \cdot K_p \cdot ZOH(s) \cdot M(s) \tag{7.25}$$

or

$$H(s) = \frac{1242.18 \cdot e^{-s\cdot 5\cdot 10^{-4}}}{s(1 + s\cdot 0.1)} \tag{7.26}$$

The phase angle of H(s) for ω_c is

$$\varphi_H = \frac{\omega_c T}{2} \cdot \frac{180°}{\pi} - 90° - \tan^{-1}(0.1\cdot 125) = -179° \tag{7.27}$$

To produce a phase margin φ_{cp} of 45° the digital filter G(z) has to produce a phase anticipation φ_D of 44°. A tentative G(s) lead-lag filter is

$$G(s) = K\frac{s + \omega_1}{s + \omega_2} \tag{7.28}$$

The maximum anticipation is obtained for $\omega_c = (\omega_1\omega_2)^{0.5}$. The filter phase angle φ_D is

$$\varphi_D = \tan^{-1}\left(\frac{\omega_c}{\omega_1}\right) - \tan^{-1}\left(\frac{\omega_c}{\omega_2}\right) \tag{7.29}$$

with ω_c = 125 rad/sec and φ_D = 44°, ω_1 = 53.3 rad/sec and ω_2 = 293.15rad/sec.

Finally, the amplification K of G(s) is obtained from the condition that the amplitude of the open-loop transfer function of the system |H(s) G(s)| be equal to unity for critical frequency. With the above data, K = 2.96.

To discretize the G(s) transfer function, the correspondence between z and s is considered

$$s = \frac{2}{T}\frac{z-1}{z+1} = 2000\frac{z-1}{z+1} \tag{7.30}$$

Consequently G(z) is

$$G(z) = 2.65\frac{z-0.947}{z-0.744} = \frac{Y(z)}{\varepsilon(z)} \tag{7.31}$$

or

$$Y(z) - 0.744 \cdot z^{-1}Y(z) = 2.65\varepsilon(z) - 2.51 \cdot z^{-1}\varepsilon(z) \tag{7.32}$$

Finally the output of the digital filter Y(k) is

$$Y(k) = 0.744 \cdot Y(k-1) + 2.65\varepsilon(k) - 2.51 \cdot \varepsilon(k-1) \tag{7.33}$$

7.2.4 Positioning precision

It is known that the positioning precision is influenced by the friction torque. Let us consider a friction torque $T_f = 0.05$Nm.

The speed is small around the target position and thus the motion induced voltage of the motor may be neglected

$$V = R \cdot I = R\frac{T_f}{K_T} = \frac{1 \cdot 0.05}{0.2} = 0.25\,V \tag{7.34}$$

The command voltage of the static power converter V_c is

$$V_c = \frac{V}{K_c} = \frac{0.25}{10} = 0.025\,V \tag{7.35}$$

The DAC input N_c is

$$N_c = \frac{V_c}{K_d} = \frac{0.025}{\frac{10}{128}} = 0.32\,\text{pulses} \tag{7.36}$$

The gain of the digital filter K_o is obtained for Z = 1

$$K_0 = 2.65\left(\frac{1-0.94}{1-0.7441}\right) = 0.548 \tag{7.37}$$

Consequently, the input of the digital filter N_e is

$$N_e = \frac{N_c}{K_0} = \frac{0.32}{0.548} = 0.584\,\text{pulses} \tag{7.38}$$

The closest integer is $N_{ei} = 1$ pulses and thus the position error $\Delta\theta_r$ caused by the above friction torque is

$$\Delta\theta_r = \frac{N_e \cdot 360^\circ}{4N} = \frac{1 \cdot 360}{2000} = 0.18^\circ \tag{7.39}$$

The positioning precision may be improved through diverse methods such as increasing the encoder number of pulses per revolution N or by a

feedforward signal proportional to the torque perturbation. Optical encoders with up to 20,000 pulses/revolution are available today.

Industrial position controllers in digital implementation are, in general, of P type but contain a speed feedforward signal and an inner PI speed-loop besides the torque loop (Figure 7.6) [4].

It should be noticed that both $\hat{\omega}_r^*$ and $\hat{\omega}_r$ — estimated reference speed and actual speed — are calculated through the position time derivative and thus contain noise and errors.

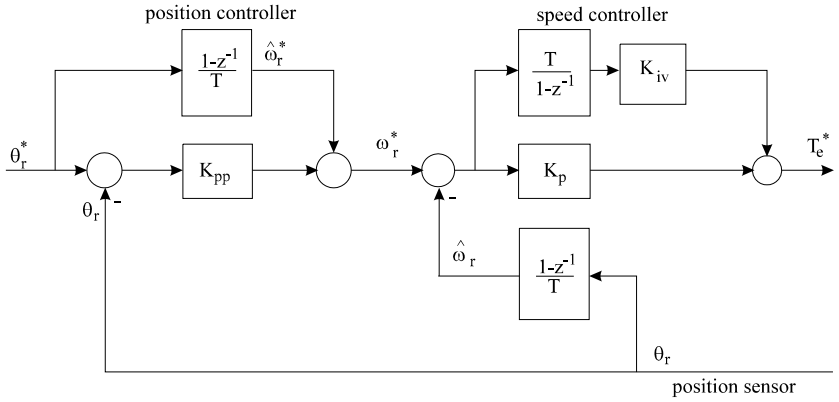

Figure 7.6. Standard digital position control system with inner speed-loop

In general such a controller responds well to slow dynamics commands, well below the frequency of the position controller (0.5 to 10 Hz). For this reason, in order to follow correctly the targeted position during transients, in the presence of torque and inertia changes, state-space control is used where the speed and acceleration are estimated adequately from the measured position.

7.3. STATE-SPACE MOTION CONTROL

State-space motion control which makes use of a few variables has the advantage that the scales are directly related to the capacity to reject torque perturbations (to mechanical rigidity). In such systems there is a separation of position tracking commands from those related to perturbation rejection. To yield zero position tracking errors a positive torque reaction is used. That does not affect the stability to perturbations but poses problems to torque dynamics and estimation precision (Figure 7.7).

It should be noted that the friction torque coefficient b_p (Figure 7.7) as well as the inertia $\hat{J}$ have to be known with good precision. The estimated

($\hat{\omega}_r$) and reference (ω_r^*) speed and the reference acceleration ($\dot{\omega}_r^*$) are all given as time functions

$$\hat{\omega}_r = \frac{\theta_r(k) - \theta_r(k-1)}{T} \tag{7.40}$$

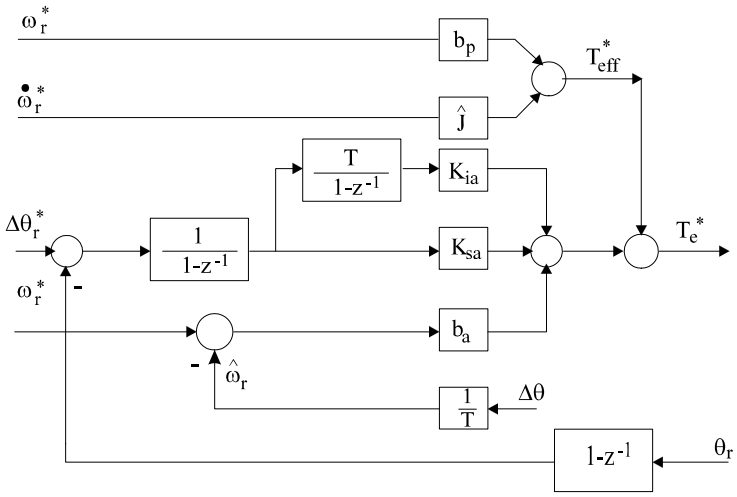

Figure 7.7. State-space position controller with zero tracking error

The speed estimation with zero delay may be done through an observer (Figure 7.8) that more complicated than the simple reference equation in (7.40).

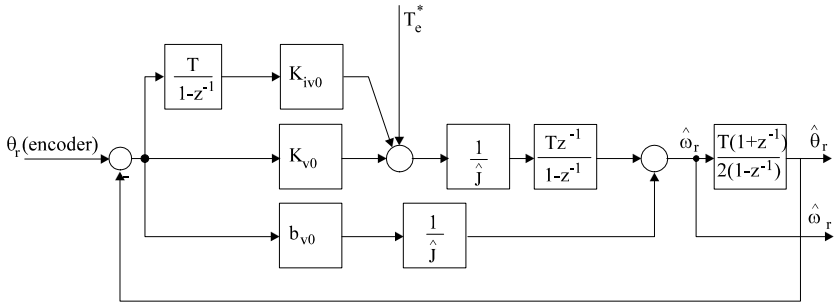

Figure 7.8. Zero delay speed observer

However, even such an observer is sensitive to torque dynamics and to torque estimation precision. The immunity to torque perturbations in position control may be further increased, especially at low speeds, through an acceleration feedback. The required acceleration observer is similar to the speed observer in Figure 7.8 but is also provided with a speed-loop whose

reference is the output of the speed observer itself. Consequently, the position control with observers and loops for speed and acceleration thus obtained (Figure 7.9) shows an increased dynamics rigidity. Even in this case problems remain related to the needed knowledge of instantaneous torque and inertia $\hat{J}$ (J_a is only an active inertia). In what follows the estimation of torque perturbations is approached.

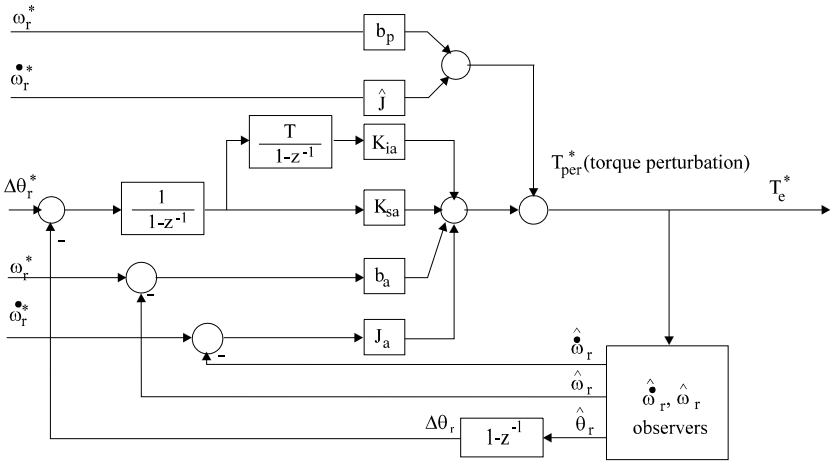

Figure 7.9. Position controller with observers and loops for speed and acceleration and reference torque feedforward signal

7.4. TORQUE PERTURBATION OBSERVERS

The response of the cascaded motion control systems, designed for given (constant) torque and rated motor parameters, proved to be strongly influenced by torque, inertia and parameter variations. Increasing the gain would make the system more rigid but it could excite low frequency mechanical resonant modes which may lead to instabilities. The reference torque feedforward signal produces similar effects. Motion control (in robotics, etc.) requires, on the other hand, even more increased dexterity and thus a variable dynamic rigidity. A robot that rotates a cam shaft requires a force loop while another that plants electronic components implies refined motion control. In these latter cases there is no urgent need for control rigidity but the robustness of response is also lost if the gains would be reduced in the standard controller. This is how a variable rigidity controller becomes necessary. To reach this goal use is made of total perturbation observers (of torque and parameters) or partial ones (of torque) [5].

To simplify the presentation a single degree of freedom system is considered. Its motion equation is

$$J\frac{d\omega_r}{dt} = T_e - T_L; \quad T_L = T_{in} + T_{L0} + T_{fr} \tag{7.41}$$

where T_{in} is the inertia torque; T_{Lo} is the load torque; and T_{fr} is the friction torque.

The electromagnetic torque of the motor T_e (of the PM d.c. brush or of vector controlled a.c. motors) has the simple expression

$$T_e = K_T \cdot I^* \tag{7.42}$$

where I^* is the reference torque current and, consequently, the torque (current) controller is considered to be hyper-rapid in response. The parameters in (7.41-7.42) are J and K_T, and they deviate from their rated values J_n and K_{Tn}

$$J = J_n + \Delta J \tag{7.43}$$

$$K_T = K_{Tn} + \Delta K_T \tag{7.44}$$

In terms of torque, the variations of ΔJ and ΔK_T are $\Delta J s\omega_r$ and $\Delta K_T I^*$, respectively. Consequently the torque perturbation T_{per} is

$$T_{per} = T_L + \Delta J s\omega_r - \Delta K_T \cdot I^* \tag{7.45}$$

Making use of (7.43)-(7.45) in (7.41) leads to

$$T_{per} = K_{Tn} \cdot I^* - J_n s\omega_r \tag{7.46}$$

Based on (7.46) the torque perturbation may be rather simply calculated. To avoid the time derivative in (7.46), a change is operated and a low pass filter added (Figure 7.10). If the critical frequency, a, of the low pass filter is sufficiently high, the estimated torque perturbation T_{per} is very close to the actual one. The torque perturbation T_{per} may also be used as a positive reaction (Figure 7.11) to replace the same quantity but recalculated with the reference values.

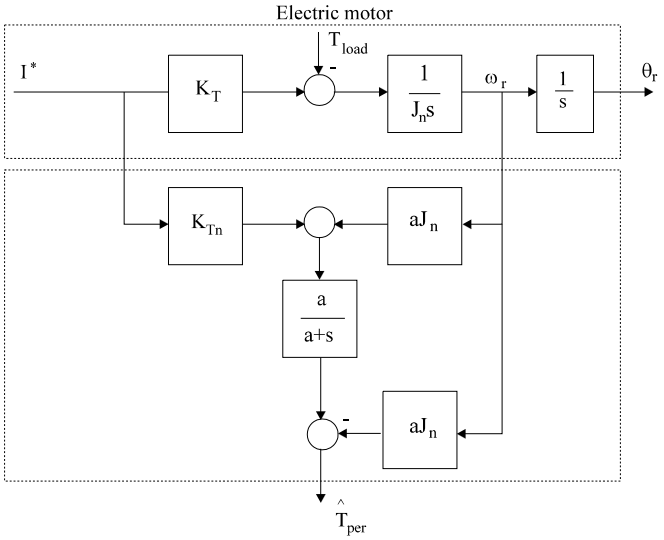

Figure 7.10. Torque perturbation estimator based on speed information

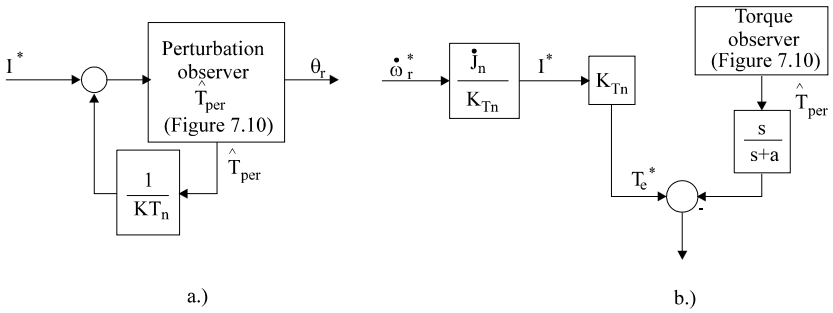

Figure 7.11. Torque perturbation reaction

a.) positive reaction; b.) negative reaction at the reference T_e^*.

7.5. PATH TRACKING

Making use of torque perturbation (T_{per}) leads to increased control rigidity and thus to the possibility of close trajectory (path) tracking. For path tracking the reference position in two (three) previous time steps is known and thus reference acceleration and speed signals may be calculated and used in the control system.

Stabilizing the position response is accomplished by at least two poles with negative real parts which could be made dependent on the gains of the position and speed-loops K_1 and K_2. This solution plus the inverse system may lead to a robust path tracking control system (Figure 7.12) — for multivariable systems.

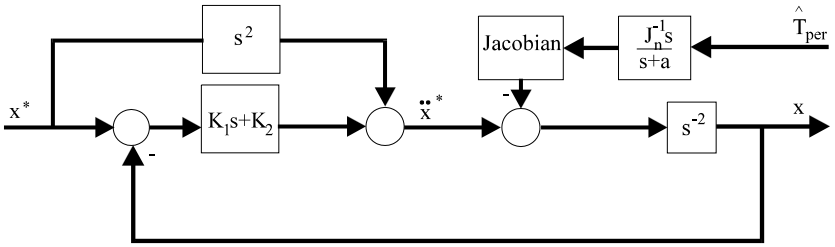

Figure 7.12. Position tracking multivariable system (J - Jacobian matrix)

The relationship between the actual and reference position (Figure 7.12) is

$$x = x^* - \text{Jacobian}\frac{s\hat{T}_{per}}{(s+a)J_n\left(s^2 + K_1 s + K_2\right)} \tag{7.47}$$

7.6. FORCE CONTROL

The above procedure may be used to control the force without its direct measurement (Figure 7.13).

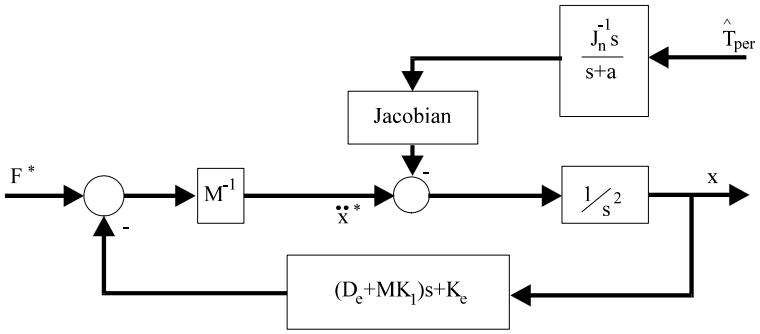

Figure 7.13. Multivariable force control

The rigidity K_e and the viscosity coefficient D_e model the medium where the force acts. The speed feedback amplification K_1 provides for stability. It may well be said that the external loop in Figure 7.13 adjusts the motion rigidity by generating the reference acceleration $\ddot{x}^*$ while the interior loop provides for force tracking, yielding a robust response.

Applying such robust motion control systems also implies, as shown above, speed calculation from the measured position [5]. Results obtained at low speed show remarkable performance (Figure 7.14) [5].

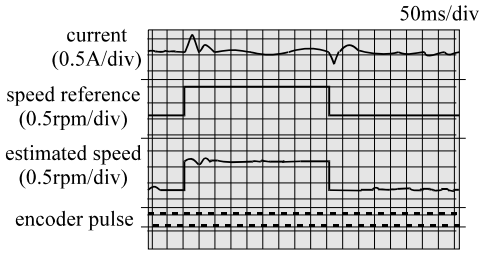

Figure 7.14. Motion control at low speeds with a speed observer with average speed input (4N = 5000 pulses / rev, with a pole z = 0.3) [5]

We should also mention that so far inertia was considered known. In reality even this parameter has to be estimated and this is why the block diagrams so far contain the estimated inertia $\hat{J}$ [4-6]. To estimate $\hat{J}$ we may use the motion equation in a few moments in time

$$J\dot{\omega}_r(k) = K_{Tn} \cdot I(k) + T_{per}(k) \tag{7.48}$$

$$J\dot{\omega}_r(k-1) = K_{Tn} \cdot I(k-1) + T_{per}(k-1) \tag{7.49}$$

Making use of the acceleration and perturbation torque estimators we may calculate — through averaging methods (such as the least-square recursive method) — in real time, the inertia. Consequently, a fully robust motion controller performance is obtained (Figure 7.15) [5].

Though the series of procedures for robust control presented under the umbrella of state-space control seems to exhaust the subject, other less complex but high performing nonlinear control methods have been proposed. Among them we will treat in some detail the variable structure (sliding-mode) systems, fuzzy control systems and neural-network control systems.

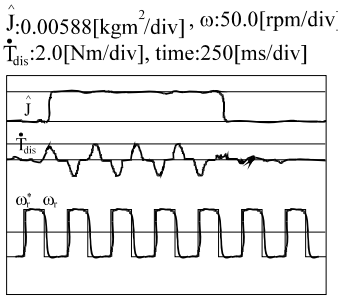

Figure 7.15. Inertia identification

(based on the time interval between encoder pulses T_2 = 100μsec,

with the speed estimation time T_1 = 5ms; observer poles: z = 0.6, M = 50) [5]

7.7. SLIDING-MODE MOTION CONTROL

Sliding-mode motion controllers force the system to move on a given surface in the state-space (plane) [7]. The simplest "surface" in the state plane is a straight line. The equation of the sliding mode functional s_s is

$$s_s = c\varepsilon - \frac{d\varepsilon}{dt};\ \ \varepsilon = x^* - x \tag{7.50}$$

where ε is the error of the controlled variable x. For $s_s = 0$ a straight line is obtained.

According to Figure 7.16, in the initial moment the system starts from point A with an error ε_i = OA and its derivative is zero. At A, $s_s > 0$. By forcing the command variable (voltage or current) in the positive direction the motor has to be capable of jumping up to the straight line $s_s = 0$.

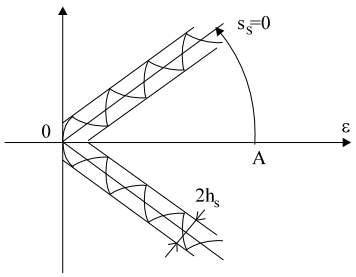

Figure 7.16. Sliding-mode functional

Once this is done, the positive and negative commands (±V) alternate depending on the sign of s_s (at a constant switching frequency or with a hysteresis band h_s) to run the system to origin where a new steady-state point is reached

$$\begin{aligned} V_c &= +V_0 \quad \text{for} \quad s_s > h_s \\ V_c &= 0 \quad \text{for} \quad |s_s| < h_s \\ V_c &= -V_0 \quad \text{for} \quad s_s < -h_s \end{aligned} \tag{7.51}$$

Such a simple forcing process done through the switching of the command variable between three discrete values leads, however, to oscillations around the target position (chattering) unless the switching frequency is high enough. The system's behavior seems to depend only on the constant c and thus only the limits within which the motor parameters and load torque vary are known in order to allow for sliding along the straight line $s_s = 0$. However the sliding-modes existence conditions have to be fulfilled also [7]

$$s_s \cdot \dot{s}_s < 0 \tag{7.52}$$

The simplifications introduced by the sliding-mode robust control seem notable but operation without chattering requires some additions such as a perturbation observer [8].

The block diagram of a motion (position) control system with sliding-modes for a robot, is shown in Figure 7.17.

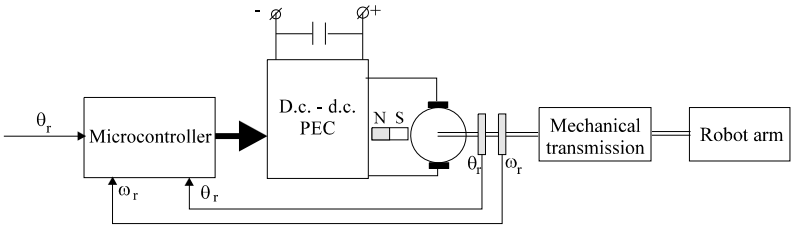

Figure 7.17. Sliding-mode motion control system for a robot arm

The mathematical model of the PM d.c. brush motor for position control, accounting for the mechanical transmission ratio K_{mT}, the friction torque coefficient D and the total load torque T_{per}, has a second order only if the motor inductance is considered zero

$$\ddot{\theta}_r = \frac{-(K_E K_T + DR)\dot{\theta}_r}{RJ} + \frac{K_E K_{mT} V_a}{RJ} - \frac{K_{mT}}{J} T_{per} \tag{7.53}$$

D - friction coefficient;
J - total inertia referred to the motor shaft;

K_E - PM motion induced voltage coefficient ($E = K_E \dot{\theta}_r$);
K_T - motor torque coefficient ($T_e = K_T I$; $K_T = \lambda_{PM}$);
V_a - motor armature voltage.
Two new variables x_1 and x_2 are introduced

$$x_1 = \overset{*}{\theta}_r - \theta_r \text{ and } x_2 = \frac{dx_1}{dt} \tag{7.54}$$

with

$$V = aV_a; \quad a = \frac{K_E K_{mT}}{JR}$$
$$b = \frac{DR + K_E K_T}{JR}; \quad f = \frac{K_{mT} T_{per}}{J} \tag{7.55}$$

Equation (7.53) becomes

$$\dot{x}_1 = x_2$$

$$\dot{x}_2 = bx_2 - V + f \tag{7.56}$$

The sliding-mode command voltage is chosen in the form [9]

$$V_c = \gamma x_1 + K_f \, \mathrm{sgn}(s_s) \tag{7.59}$$

with

$$\gamma = \begin{cases} \alpha \ \text{if} \ s_s x_1 > 0 \\ \beta \ \text{if} \ s_s x_1 < 0 \end{cases} \tag{7.60}$$

The state functional is given by (7.50) while the sliding-mode existence condition is given by (7.52). The existence condition (7.52) leads to the inequalities

$$\alpha > c(b - c) \tag{7.61}$$

$$\beta < c(b - c) \tag{7.62}$$

$$K_f > (f)_{max} \tag{7.63}$$

These conditions secure safe jumping of the system to the straight line of the sliding-mode functional. We call K_f a dither signal, and it should be greater than a quantity proportional to the largest torque perturbation. Unfortunately once the straight line is reached, the term in K_f in the command voltage (7.59) causes undesirable vibrations.

Figures (7.18-7.19) show results obtained with such a control system implemented on a DSP (NEC: μPD77230, 32 bit) with a sampling time of 200μs, 20kHz switching frequency, for a SCARA robot with two axes [8].

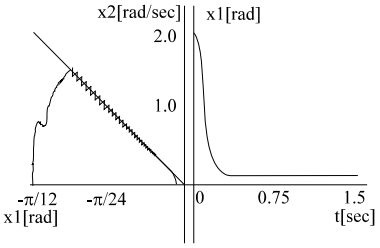

Figure 7.18. Sliding-mode control (7.59) with low K_f

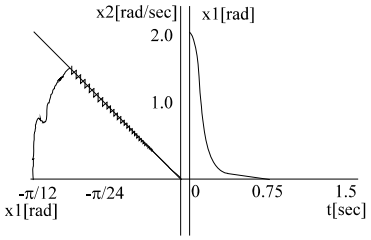

Figure 7.19. Sliding-mode control with large K_f

The perturbation, which in the first case (K_f small, Figure 7.18) produces a nonzero steady-state position error, is caused by pulling down the robot arm with 300g through a spring (about 20% loading). The undesirable mechanical vibrations are notable. Elimination of such vibrations is accomplished through the contribution of a perturbation observer with a reduction of K_f. If stepwise perturbations are assumed, the equations are:

$$\begin{aligned} \dot{T}_{per} &= 0 \\ \dot{x}_2 &= \frac{K_{mT} T_{per}}{J} - b\hat{x}_2 - V \end{aligned} \tag{7.64}$$

It may be proved that the system of (7.64) is observable and, to calculate (observe) T_{per} and x_2, a complete observer may be used

$$\dot{\hat{T}}_{per} = K_1\left(x_2 - \hat{x}_2\right) \tag{7.65}$$

$$\dot{\hat{x}}_2 = \frac{K_{mT}\hat{T}_{per}}{J} - b\hat{x}_2 - V + K_2\left(x_2 - \hat{x}_2\right) \tag{7.66}$$

The two amplifications K_1 and K_2 may be calculated by the method of pole allocation. Complex poles with negative real part are assumed. The positive perturbation reaction V_0 becomes

$$V_0 = \frac{K_{mT} T_{per}}{J} \tag{7.67}$$

Finally, the complete command voltage Vcc is

$$V_{cc} = V_c + V_0 = \gamma x_1 + K_f \operatorname{sgn}(s_s) + V_0 \tag{7.68}$$

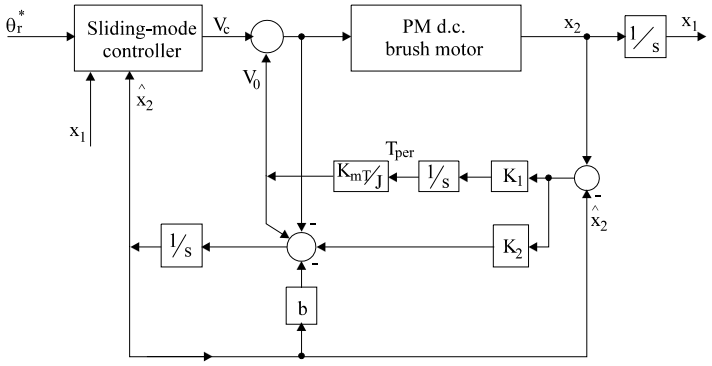

Figure 7.20. Sliding-mode position control with perturbation feedforward signal

The stability of such a nonlinear system may be studied through Lyapunov's theorem. A Lyapunov function, $V(s_s, \Delta x_2, \Delta T_{per})$, is first defined as

$$V\left(s_s, \Delta x_2, \Delta T_{per}\right) = \frac{1}{2} s_s^{\,2} + \frac{1}{2}\left[\frac{1}{K_1}\left(\Delta T_{per}\right)^2 + \frac{J}{K_{mT}}\left(\Delta x_2\right)^2\right] \tag{7.69}$$

The sufficient condition for stability is satisfied if $\dot{V} < 0$

$$\dot{V} = (c-b)\left|\hat{s}_s\right|^2 - \left[c(c-b)+\gamma\right]\hat{s}_s\,\Delta\hat{x}_1 -$$
$$-\left[K_f - K_2\Delta\hat{x}_2\,\mathrm{sgn}\left(\hat{s}_s\right)\right]\left|\hat{s}_s\right| - \left(b+K_2\right)\frac{J}{K_{mT}}\left(\Delta\hat{x}_2\right)^2 < 0 \tag{7.70}$$

If each term in (7.70) is negative, then $\dot{V} < 0$

$$\begin{aligned} c \le b; \qquad & \alpha > c(b-c) \\ \beta < c(b-c); \qquad & K_f > K_2\left|\Delta\hat{x}_2\right|_{max} \\ K_1 > 0; \qquad & K_2 > -b \end{aligned} \tag{7.71}$$

In case of a high step-torque perturbation ($K_{mT}T_{per}/J = 0.15$, $K_f = 0.01$), K_f becomes too small to fulfill (7.71) and thus the controller regains stability only after Δx_2 increases notably (Figure 7.21) [8].

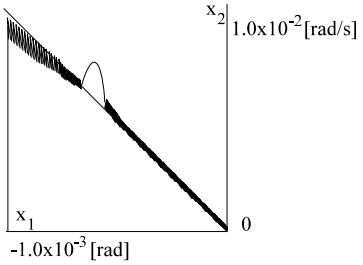

Figure 7.21. System response to step-wise perturbation ($K_{mT}T_{per}$ / J = 0.15, K_f = 0.01)

Because the perturbation observer is of the step-form a ramp perturbation causes errors in the estimated speed x_2 and thus the last two stability conditions in (7.71) have to be reformulated as [8]

$$K_f > \frac{K_2}{K_1} T_{per}^{ramp}; \quad T_{per}^{ramp}(s) = \frac{T_{per}^{ramp}}{s} \tag{7.72}$$

The stability analysis for this case leads to new conditions related to K_f

$$cT < 1 \tag{7.73}$$

$$TK_f < \left| c\hat{x}_1(k+1) + \hat{x}_2(k+1) \right| \tag{7.74}$$

The same control system may be extended to position tracking when the reference position, speed and acceleration, θ_r^*, $\dot{\theta}_r^*$, $\ddot{\theta}_r^*$ are known time functions. In this case we invert the system (7.54) with (7.55)-(7.56)

$$V = \frac{1}{a}\left(b\dot{\theta}_r + \ddot{\theta}_r^* + hx_2 + V_{cc} \right) \tag{7.75}$$

Comparing (7.53) with (7.75) yields:

$$\dot{x}_2 = -hx_2 - V_{cc} + \frac{K_{mT}T_{per}}{J} \tag{7.76}$$

Eqn. (7.75) represents the new control law which embeds (7.68) and adds three new terms for good path tracking. Figure 7.22 presents a triangle drawn by the robot SCARA (as a plotter) in the presence of a 20% torque perturbation (obtained through 200g hanged on the robot arm through a mechanical spring).

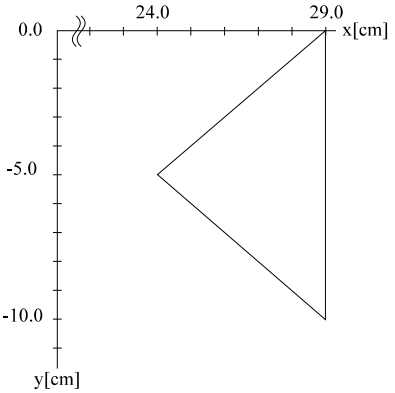

Figure 7.22. Triangular trajectory in the presence of a 20% torque perturbation

The maximum speed is 0.5m/sec [8], a = 2550, b = –2550, c = 40, h = 100, the observer poles are $p_{1,2} = Lb(-\cos\gamma + j\sin\gamma)$ with L = 30, $\gamma = 30°$.

Practical experience has shown that if in the trajectory planning high accelerations (θ_r^*) are allowed, vibrations occur in the system's response. A quadratic function E, to minimize along the trajectory, may be chosen [9]

$$E = \int_0^t \left\{ \left[f(x,y) \right]^2 + A_1 \left(\ddot{\theta}_{r1}^{\,*} \right)^2 + A_2 \left(\ddot{\theta}_{r2}^{\,*} \right)^2 \right\} J \cdot dt$$

$$A_1 > 0; \quad A_2 > 0 \tag{7.77}$$

with

$$x = L_1 \cos\theta_{r1}^{\,*} + L_2 \cos\left(\theta_{r1}^{\,*} + \theta_{r2}^{\,*} \right) \tag{7.78}$$

$$y = L_1 \sin\theta_{r1}^{\,*} + L_2 \sin\left(\theta_{r1}^{\,*} + \theta_{r2}^{\,*} \right) \tag{7.79}$$

where f(x,y) is the required trajectory in plane.

The scope of the optimization process is to determine $\theta_{r1}^{\,*}$, $\dot{\theta}_{r1}^{\,*}$, $\ddot{\theta}_{r1}^{\,*}$ and $\theta_{r2}^{\,*}$, $\dot{\theta}_{r2}^{\,*}$, $\ddot{\theta}_{r2}^{\,*}$ along the two axes as time functions such that the penalty function is minimum. Through variational methods combined with spline trajectory approximations, the above problem may be solved iteratively. Figure 7.23 shows the results obtained with SCARA robot in drawing a circle without and with acceleration reduction [8].

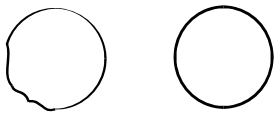

Figure 7.23. The circle drawn by SCARA robot without and with the reduction of reference acceleration (total time 1.6 sec.)

Far from exhausting the subject, the sliding-mode motion control with torque perturbation compensation, as applied to robotics, merely suggests the complexity of motion robust control even with the motor electrical time constant (constants) considered zero.

For systems with vague mathematical models, new motion control systems such as fuzzy systems and neural network systems have been recently proposed. Their first implementation has been done on PM d.c. brush motors [10] and on a.c. motors [11, 12].

7.8. MOTION CONTROL BY FUZZY SYSTEMS

Fuzzy systems stem from a logic which treats vaguely known plants by membership functions (MF) with values between 0 and 1.

In fuzzy sets, based on fuzzy logic, an object (variable) has a membership degree to a given set with values between 0 and 1.

A fuzzy variable has linguistic values, for example, LOW, MEDIUM, HIGH which may be defined through bell shape (Gauss) membership functions with gradual variation (Figure 7.24).

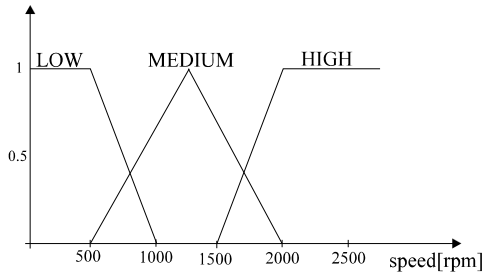

Figure 7.24. Fuzzy sets defined through membership functions

The membership functions are, in general, either symmetric or nonsymmetric, triangular or trapezoidal.

At 800rpm (Figure 7.24), for example, the variable belongs with 50% (MF = 0.5) to LOW and with 50% (MF = 0.5) to MEDIUM. All possible values of a variable constitute the universe of discourse.

The properties of Boolean theory remain valid for fuzzy sets. Reunion (corresponding to OR) is

$$\mu_{A\cup B}(x) = \max\left[\mu_A(x), \mu_B(x)\right] \tag{7.80}$$

Intersection (corresponding to AND) writes

$$\mu_{A\cap B}(x) = \min\left[\mu_A(x), \mu_B(x)\right] \tag{7.81}$$

The negation (corresponding to NOT) is

$$\mu_A(x)+\mu_{\Gamma A}(x)=1 \tag{7.82}$$

Triangular membership functions OR, AND and NOT are illustrated in Figure 7.25.

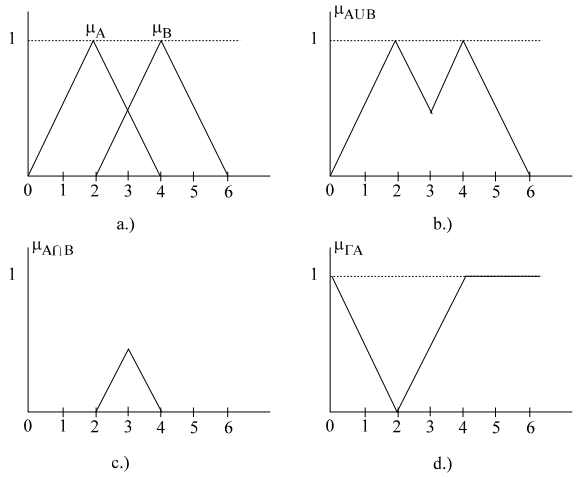

Figure 7.25. a.) Fuzzy sets A and B; b.) reunion; c.) intersection; d.) negation

While conventional control systems are based on the mathematical model of the plant, fuzzy control is based on the intuition and experience of the human operator. And thus, besides self-tuning adaptive systems, reference model adaptive systems, variable structure systems, for plants with vaguely known model, fuzzy control is clearly opportune and adequate.

In essence, implicitly, fuzzy motion control is self-adaptive and thus its robustness becomes apparent.

The command law in fuzzy systems is of the form

$$\text{IF } x = A \text{ AND } y = B \text{ THEN } z = C \tag{7.83}$$

where x, y, z are fuzzy variables where the universe of discourse is A, B, C. For example, for the speed control of a PM d.c. brush motor, the fuzzy variables are the speed error $E = \omega_r^* - \omega_r$ and its derivative $CE=\dot{\omega}_r^* - \dot{\omega}_r$. Let us remember that the same variables have been used to express the sliding-mode functional. The rule number one may be of the form: if E is zero (ZE) and the error derivative CE is negative small (NS), then the increment dV_1 of the command voltage is negative small (NS).

The linguistic variables ZE, NS and ΔV are defined through membership symmetric functions (Figure 7.26).

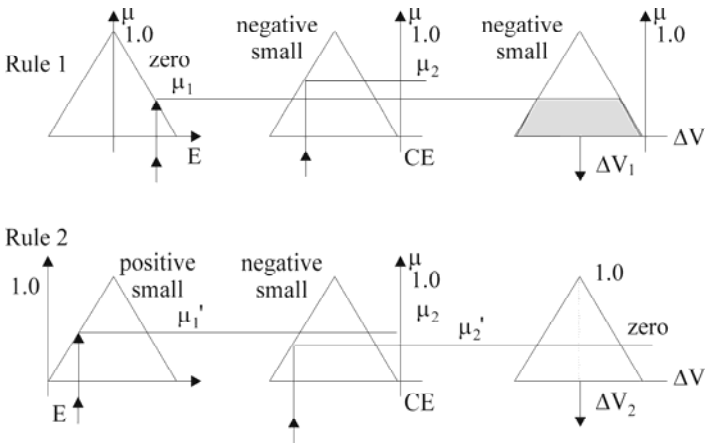

Figure 7.26. The MAX-MIN (SUP-MIN) Fuzzy rule composition

The command law ΔV_1 may be obtained graphically, but two rules may emerge, the second with the output ΔV_2. The effective control will be an average between two outputs ΔV_1 and ΔV_2. First a basis of fuzzy rules is usually constituted (Table 7.1) and the corresponding membership functions are described (Figure 7.27).

Table 7.1.

CE \ E	NB	NM	NS	Z	PS	PM	PB
NB	NVB	NVB	NVB	NB	NM	NS	Z
NM	NVB	NVB	NB	NM	NS	Z	PS
NS	NVB	NB	NM	NS	Z	PS	PM
Z	NB	NM	NS	Z	PS	PM	PB
PS	NM	NS	Z	PS	PM	PB	PVB
PM	NS	Z	PS	PM	PB	PVB	PVB
PB	Z	PS	PM	PB	PVB	PVB	PVB

Z - zero, PS - positive small, PM - positive medium, PB - positive big, PVB - positive very big
NS - negative small, NM - negative medium, NB - negative big, NVB - negative very big

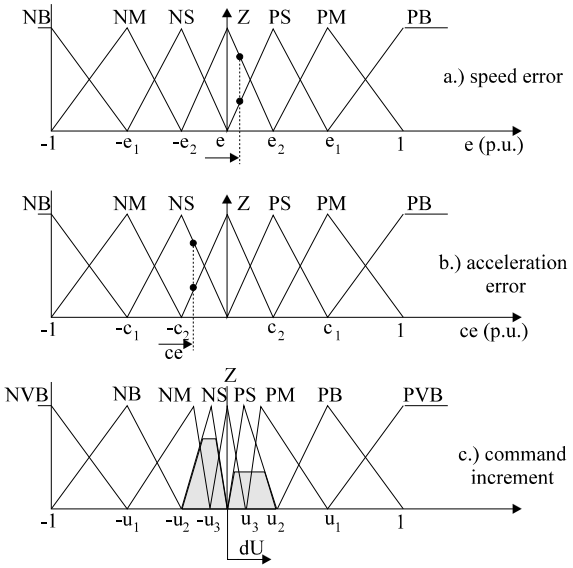

Figure 7.27. The fuzzy membership functions for speed control

The composition operation refers to the calculus of the command law. Among the composition methods we mention the MAX-MIN (SUP MIN) and MAX-DOT. The MAX-MIN method already illustrated in Figure 7.26 is written in the form

$$\mu_u(u) = \mathrm{SUP}_x\left[\min \mu_x(x) \cdot \mu_R(x,u)\right] \tag{7.84}$$

Consequently, the membership function for each rule is given by the minimum value (MIN) and the combined output is given by the supreme maximum of all rules. The general structure of a single input fuzzy motion controller is given in Figure 7.28.

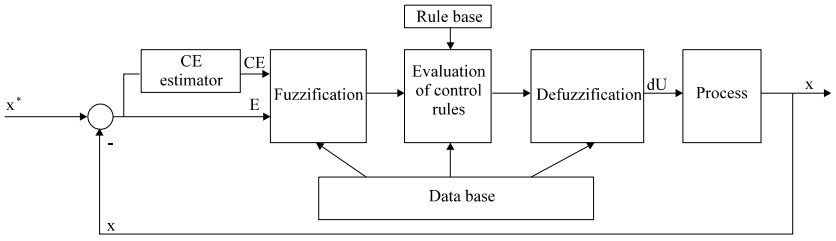

Figure 7.28. Typical single input fuzzy control system

The command variable (voltage or current in our example) is determined based on the two variables e and ce (in relative values) calculated from the

absolute values E and CE by division through the corresponding amplifications.

Fuzzification may be done by taking definite values of the variables to calculate the membership function in these cases (Figures 7.26-7.27). Defuzzification may be done in quite a few ways one of which is the centroid method by which the command variable U_o is obtained through the gravity center of the fuzzy function U (Figure 7.26).

$$U_0 = \frac{\int U\mu_u(u)\cdot du}{\int \mu_u(u)\cdot du} \tag{7.85}$$

and the height method, where the centroid of each function first and, then, a weighted medium value of the heights is calculated

$$U_0 = \frac{\sum_{i=1}^{n} U_i \mu_u(u_i)}{\sum_{i=1}^{n} \mu_u(u_i)} \tag{7.86}$$

Though the fuzzy control looks simple, mathematical implication increases the implementation time. Recently neural-fuzzy sets that allow the rapid selection of the membership functions, rules and command signals have been introduced.

Besides the rule-based method (for fuzzy systems) a relational method has been proposed in [12]. According to the relational method, regions look for linear combinations of input functions with G and H values.

The rule number one may be defined: IF W is MEDIUM and H is MEDIUM, then

$$I_s = A_{01} + A_{11}W + A_{21}H \tag{7.87}$$

The coefficients A_{ij} may be determined through linear regression and then adjusted through observation and simulation. Finally the linear equation of the outputs (7.87) is defuzzified, that is a weighted average of the components I_{s1} and I_{s2} by the membership functions μ_1 and μ_2 is calculated

$$I_s = \frac{I_{s1}\mu_1 + I_{s2}\mu_2}{\mu_1 + \mu_2} \tag{7.88}$$

To control the speed of a PM d.c. brush motor (with the rule based method, Table 7.1) the command signal is

$$U(k) = U(k-1) + GU\cdot du \tag{7.89}$$

where GU is the voltage amplification and du the command voltage increment expressed in relative values and calculated during defuzzification through the height method. For a PM d.c. brush motor of 1.84kW, 1800rpm, J = 0.0465 kgm^2, R = 0.6 Ω, L = 8 mH, K_E = 0.55 V sec/rad, $T_s = k_L\omega_r^2$, K_T =

2.78 x 10^{-4} Nm sec^2/rad, the system's response to a step perturbation (Figure 7.29) and to a step-torque increase in inertia (Figure 7.30) demonstrates a remarkable robustness.

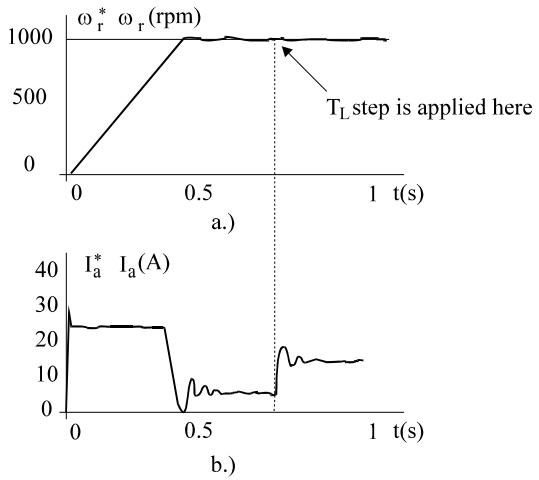

Figure 7.29. A fuzzy controller; the response to torque perturbation after step speed response: a.) speed, b.) current [10].

If for high speeds the performance is good, at low speed problems could occur and may be solved through a new set of fuzzy rules and commands.

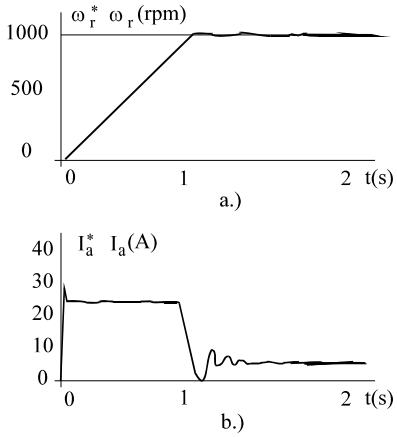

Figure 7.30. Fuzzy speed controller; the response to inertia variation: a.) speed, b.) current [10]

7.9. MOTION CONTROL THROUGH NEURAL NETWORKS

Neural networks (NN) represent systems of interconnections between artificial neurons which emulate the neuron system of the human brain. NN constitutes a more general form of artificial intelligence than the expert systems or fuzzy sets [11]. The model of an artificial neuron looks as in Figure 7.31.

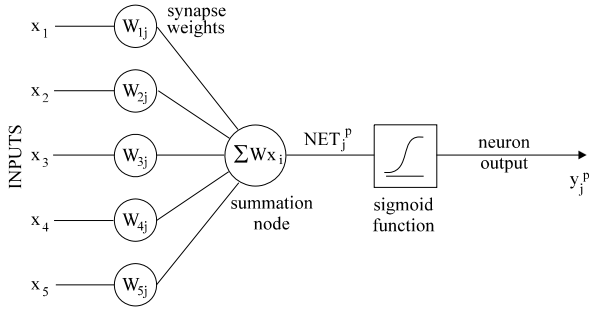

Figure 7.31. The structure of an artificial neuron

Each input continuous signal is passed through weighting synapses — positive (exciters) or negative (inhibiters) — towards the summation mode, then, through a nonlinear transfer function, to output. The transfer function may be step-wise, limit form, sign form (sgn), linear with a limit or nonlinear, of the sigmoid form, for example

$$y = \frac{1}{1 + e^{-\alpha_s x}} \tag{7.90}$$

For large α_s y gets close to a step function and varies between zero (for x = $-\infty$) to 1 (for x = $+\infty$). Though it is still a mystery how the neurons are interconnected in the human brain, more than sixty models of artificial neural networks have been proposed to be applied in science and technology. They may be classified in neural networks with positive and negative reaction. The first ones are dominant so far. Such a positive reaction model with three layers — input, hidden (screened) and output — is shown on Figure 7.32.

The relationships between the input and output variables are of the form

$$[V]_b = [W]_{ba}[X]_a \tag{7.91}$$

$$[Y]_c = [W]_{cb}[V]_b \tag{7.92}$$

The twenty-five weights $W_{i,j}$ (on Figure7.32) have to be calculated through an iterative educational process by comparing a large number of desired types of output signals with the actual ones.

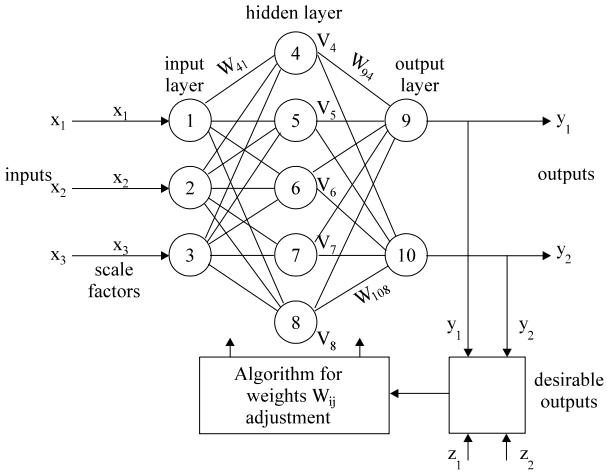

Figure 7.32. Positive reaction neural model

The back propagation educational algorithm, which has received rather wide acceptance lately, starts with a few initial values and, based on a penalty function (such as the minimum of the sum of squared errors), continues through the descent gradient method and changes the weights $W_{i,j}$.

For the case of a single layer (Figure7.31) the network equations, based on (7.91) - (7.92), become

$$NET_j^p = \sum_1^N W_{ij} X_i \tag{7.93}$$

$$Y_i^p = f_i\left(NET_j^p\right) \tag{7.94}$$

For the p^{th} input signal, the squared error E_p for all the neurons of input layer is

$$E_p = \frac{1}{2}\left(d^p - y^p\right)^2 = \frac{1}{2}\sum_{j=1}^{s}\left(d_j^{\,p} - y_j^{\,p}\right)^2 \tag{7.95}$$

For all the input signals the resultant error E is

$$E = \sum_{p=1}^{p} E_p = \frac{1}{2}\sum_{p=1}^{p}\sum_{j=1}^{s}\left(d_j^{\,p} - y_j^{\,p}\right)^2 \tag{7.96}$$

The weights $W_{i,j}$ will be reduced until E reaches a minimum

$$W_{ij}(t+1) = W_{ij}(t) + \eta\left(\frac{\partial E_p}{\partial W_{ij}(t)}\right) + \alpha\left[W_{ij}(t) - W_{ij}(t-1)\right] \tag{7.97}$$

The iterative procedure propagates the error backwards and provides for a global minimum by adequately choosing the educational rate η and the coefficient α

$$\eta(t+1) = U \cdot \eta(t); \quad U > 0 \tag{7.98}$$

Special education algorithms with back propagation are now available.

7.10. NEURO-FUZZY NETWORKS

The neuro-fuzzy networks do the calculations, required in the fuzzy systems, by the rule-based or relational methods through which the rules and membership functions are identified.

For the fuzzy speed control (Figure7.27) a neuro-fuzzy network is given in Figure 7.33.

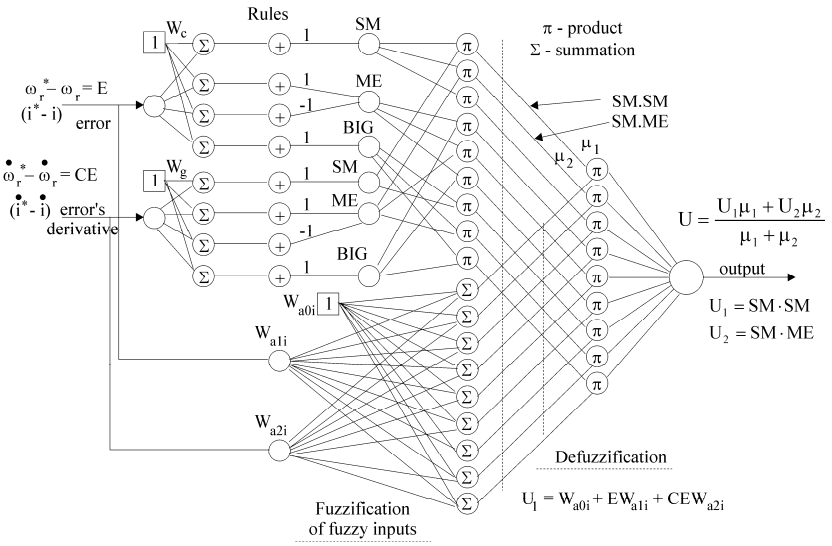

Figure 7.33. A neuro-fuzzy speed controller

In essence, the fuzzy control, with the relational method used for command signal calculation, is done through the neuro-fuzzy controller. The quantities W_c and W_g create the space between the membership functions and, respectively, their ramp. Nine rules occur. The linear functions (for the relational method) are given on the lower part of Figure 7.33 while defuzzification is shown on the right side of the same figure.

Besides positive reaction, negative reaction neural networks [14] have been proposed.

7.10.1. Applications of neural networks

It is also possible to use NN (neural networks) to selectively eliminate harmonics for pulse width modulation in static power converters in the sense that the NN may be educated through the voltage chopping angles. Education of NN may be done "on line" or "off line" with applications in diagnosis and monitoring and in intelligent motion control. Also flux linkage, torque, or active power may be estimated through NN, based on measured voltages and currents [15]. Other applications include a.c. current controllers for a.c. motors [16] or d.c. brush motor control [17].

The NN may be implemented through software in microcontrollers or on special hardware. A few dedicated IC chips for the scope are already on the market such as INTEL 8017 NxETANN, Microdevice MD 1220NBS and Neural Semiconductor NUSU32.

7.11. SUMMARY

- This chapter presented a synthesis of classical — cascaded — and of nonlinear motion closed-loop control systems for electrical drives.
- The cascaded-torque, speed controllers are presented in detail with the PECs simulated by simple gains.
- The digital position controller performed through a single digital filter is illustrated by an example where the PEC is simulated by a gain and a zero order hold.
- The nonlinear motion control systems — a science in itself — is introduced here only through a few methods such as: state-space control with torque and speed observers, sliding mode control, fuzzy control, and neural networks control with recent results from literature, all related to the PM d.c. brush motor drives. Our introduction to this subject is only a starting point for the interested reader who should pursue the selected literature at the end of this chapter.
- Though applied only to d.c. brush motors the issues in this chapter are far more general and may be applied to vector-controlled a.c. motors.

7.12. PROBLEMS

7.1. Calculate the response of the current controller in Section 7.2.1 for a step increase of reference current of 10A.

7.2. A d.c. brush motor with the data $R_a = 0.25\ \Omega$, rated current 20 A, rated (source) voltage $e_0 = 110$ V, rated speed $n_n = 1800$ rpm is fed through a power transistor chopper in the continuous (constant) current mode. The inertia J = 0.1 kgm2. The mechanical time constant $\tau_m = 2\pi J/B = 10$ sec. The electrical time constant $\tau_e = 40$ ms and thus the electrical phenomena are much faster than the mechanical ones. The drive has a proportional (P) current controller with a current sensor having $K_I = 0.5$ V/A ratio and a PI speed controller. Design the speed controller — find

K_{sn} and τ_{sn} — for a damping ratio of $1 / \sqrt{2}$ and a natural frequency ω_n = 10rad/s. The speed sensor gain is $K_n = 0.1$ Vs/rot.

7.3. For the speed controller d.c. brush motor system in problem 7.2 find the speed-load torque function and show that the steady-state error in speed to a torque perturbation is zero.

7.4. A d.c. brush series motor has the data: total (armature + field) resistance $R_{at} = 1\ \Omega$, total inductance $L_{at} = 40$ mH, rated voltage $V_n = 120$ V, rated speed $n_n = 1800$ rpm, rated current 10 A. The remnant flux induced voltage at rated speed is $e_{rem} = 5$ V and the magnetizing curve is otherwise linear and $J = 10^{-2}$ kgm^2.

a. Determine the open-loop transfer functions $i_a(p) / e_a(p)$, $n(p) / i_a(p)$ for zero load torque variation, after linearization around the rated point (e_a - terminal voltage).

b. Determine the open-loop transfer functions $i_a(p) / T_L(p)$, $n(p) / i_a(p)$ for zero input voltage variation, after linearization around the rated point.

7.13. SELECTED REFERENCES

1. **B. Kisacanin, G.C. Agarwal,** Linear Control Systems, Kluwer Academic Press, 2001
2. **P. Katz,** Digital Control Systems Using Microprocessors, Prentice Hall, 1982
3. **H.F. Vanlandingham,** Introduction to Digital Control Systems, Macmillan, 1985
4. **R. Lorenz, T.A. Lipo, D.W. Novotny,** Motion Control with Induction Motors, IEEE Proc., vol.82, no.8, 1994, pp.1215-1240
5. **K. Ohnishi, N. Matsui, Y. Hori,** Estimation, Identification and Sensorless Control in Motion Control Systems, IBID., pp.1253-1265
6. **I. Awaya** et al, New Motion Control With Inertia Identification Using Disturbance Observer Record of IEEE - IECON 1992, vol.1, pp.77-80
7. **V.I. Utkin,** Variable Structure System With Sliding Mode, IEEE Trans., vol.AC - 27, no.2, 1977, pp.212-222
8. **A Kawamura, H. Itoh, K. Sakamoto,** Chattering Reduction of Disturbance Observer Based Sliding Mode Control, IEEE Trans., vol.IA - 30, no.2, 1994, pp.456-461
9. **K. Sakamoto, A. Kawamura,** Trajectory Planning Using Optimum Solution of Variational Problem, Power Conversion Conference, Yokohama 1993, pp.666-671
10. **G.D. Sousa, B.K. Bose,** A Fuzzy Set Theory Based Control of a Phase - Controlled Converter D.C. Machine Drive, IEEE Trans., vol.IA - 30, no.1, 1994, pp.34-44
11. **B.K. Bose,** Expert System, Fuzzy Logic And Neural Network Applications in Power Electronics and Motion Control, IEEE Proc., vol.82, no.8, 1994, pp.1303-1323
12. **T. Takagi, M. Sugero,** Fuzzy Identification Systems and Its Applications to Modeling and Control, IEEE Trans., vol.SMC - 15, no1, 1985, pp.116-132
13. **L.A. Zadeh,** Fuzzy Sets, Informat. Contr., vol.8, 1965, pp.338-343
14. **California Scientific Software,** Introduction to Neural Networks, Grass Valley CA, 1991
15. **M.G. Simoes, B.K. Bose,** Feedback Signal Estimation by Neural Network, Record of IEEE - IAS - 1994 Annual Meeting;
16. **M.R. Buhland, R.D. Lorenz,** Design and Implementation of Neural Networks for Digital Current Regulation of Inverter Drive, Record of IEEE-IAS - 1991 Annual Meeting, Part 1, pp.415-423
17. **S. Weerasooriya, M.A. El-Sharkawi,** Identification and Control of a D.C. Motor Using Back - Propagation Neural Networks, IEEE Trans., vol.EC - 6, no.6, 1991, pp.663-669.